Visualizing the three-dimensional arrangement of hydrogen atoms in organic molecules by Coulomb explosion imaging

Alice E. Green,[1,2,3,*] Keyu Chen,[4,†] Surjendu Bhattacharyya,[4,1] Felix Allum,[1,5] Sergey Usenko,[2] Michael N. R. Ashfold,[6] Thomas M. Baumann,[2] Kurtis D. Borne,[4,1] Mark Brouard,[7] Michael Burt,[7] Basile F. E. Curchod,[6] Benjamin Erk,[5] Ruaridh J. G. Forbes,[1] Lea M. Ibele,[8] Rebecca A. Ingle,[9] Huynh Van Sa Lam,[4] Xiang Li,[1] Kang Lin,[10] Tommaso Mazza,[2] Joseph W. McManus,[7] Michael Meyer,[2] Terrence Mullins,[2] Joao Pedro Figueira Nunes,[11] Daniel Rivas,[2] Aljoscha Roerig,[2] Arnaud Rouzée,[12] Philipp Schmidt,[2] John Searles,[4] Björn Senfftleben,[2] Henrik Stapelfeldt,[13] Rico Mayro P. Tanyag,[13] Florian Trinter,[14] Anbu Selvam Venkatachalam,[4] Enliang Wang,[4] Emily M. Warne,[7] Peter M. Weber,[15] Thomas J. A. Wolf,[1] Till Jahnke,[2,16] Artem Rudenko,[4] Rebecca Boll,[2,‡] and Daniel Rolles[4,§]

[1] *SLAC National Accelerator Laboratory, Menlo Park, California 94025, USA*
[2] *European XFEL, Holzkoppel 4, 22869 Schenefeld, Germany*
[3] *EaStCHEM School of Chemistry, University of Edinburgh, Edinburgh EH9 3FJ, United Kingdom*
[4] *James R. Macdonald Laboratory, Physics Department, Kansas State University, Manhattan, KS 66506, USA*
[5] *Deutsches Elektronen-Synchrotron DESY, Notkestrasse 85, 22607 Hamburg, Germany*
[6] *School of Chemistry, Cantock's Close, University of Bristol, Bristol, BS8 1TS, UK*
[7] *Chemistry Research Laboratory, Department of Chemistry, University of Oxford, Oxford OX1 3TA, UK*
[8] *Aix Marseille University, CNRS, ICR, 13397 Marseille, France*
[9] *Department of Chemistry, University College London, London, WC1H 0AJ, UK*
[10] *Institut für Kernphysik, Goethe-Universität Frankfurt, Max-von-Laue-Str. 1, 60438 Frankfurt am Main, Germany*
[11] *Diamond Light Source Ltd, Didcot, OX11 0DE, UK*
[12] *Max-Born-Institut, Max Born Straße 2A, 12489 Berlin, Germany*
[13] *Department of Chemistry, Aarhus University, Langelandsgade 140, DK-8000 Aarhus C, Denmark*
[14] *Molecular Physics, Fritz-Haber-Institut der Max-Planck-Gesellschaft, Faradayweg 4-6, 14195 Berlin, Germany*
[15] *Department of Chemistry, Brown University, Providence, RI, USA*
[16] *Max-Planck-Institut für Kernphysik, 69117 Heidelberg, Germany*

* alice.green@ed.ac.uk
† both authors (Green and Chen) have contributed equally to this work
‡ rebecca.boll@xfel.eu
§ rolles@ksu.edu

I. ALTERNATIVE DATA REPRESENTATIONS

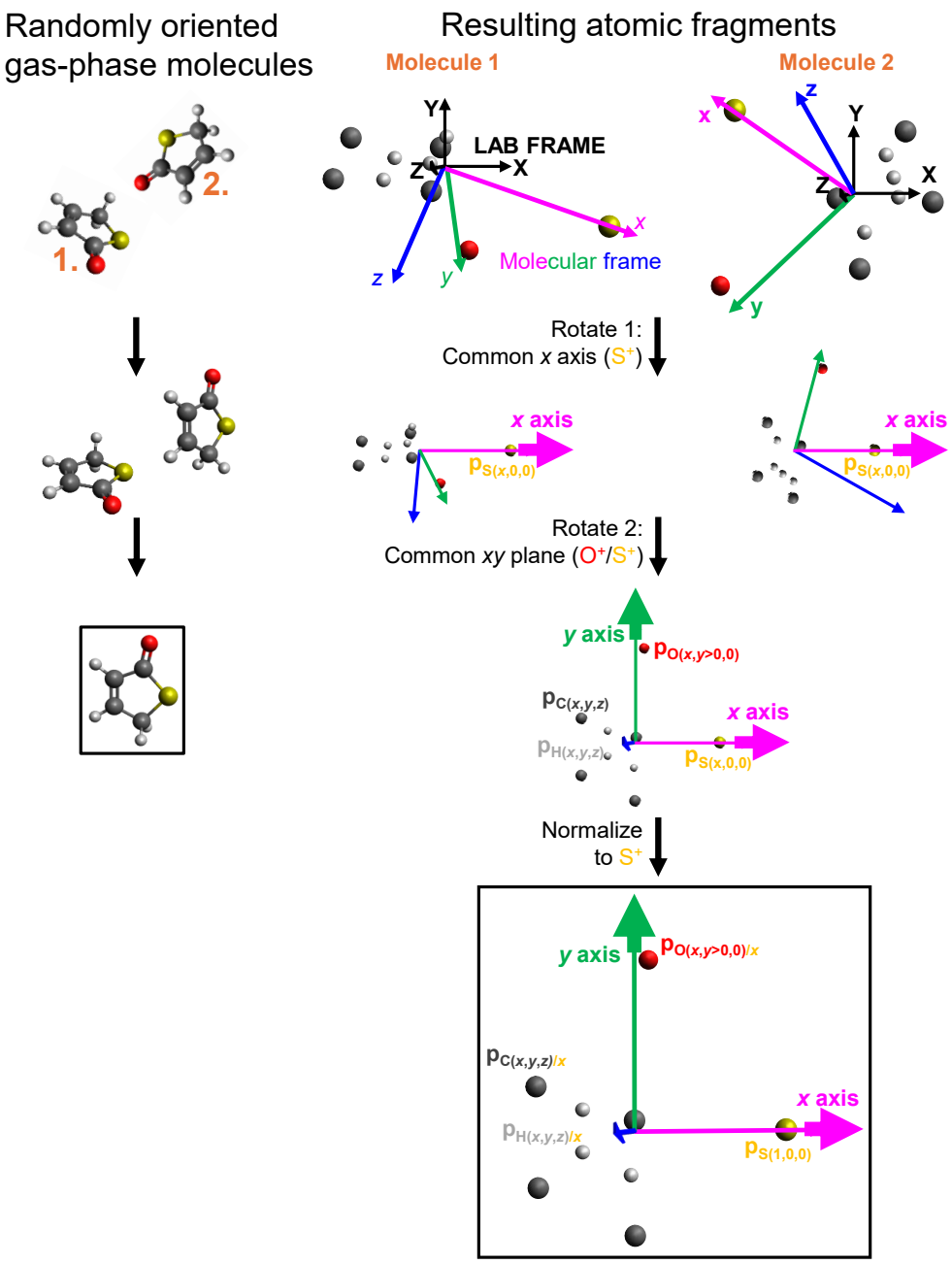

FIG. 1. Schematic of the chosen molecular frame used for presenting Coulomb explosion data within the main text. On a shot-by-shot basis, we can align the momenta of these sets of ions detected together onto a common orientation (molecular frame given by the coloured arrows) for all shots and acquire this molecular-frame Coulomb explosion image over a large dataset. Here, this coordinate frame is chosen such that the S^+ momentum points along the positive x axis and the O^+ momentum spans the xy plane (with $p_y > 0$). One of these ions or a third particle (H^+ or C^+) is then plotted within this frame. The magnitude of each momentum is normalized by the magnitude of the S^+ momentum. All S^+ ions therefore have momentum coordinates (1,0,0), all O^+ ions (p_x,p_y > 0,0), and all H^+ and C^+ coordinates are transformed relative to this.

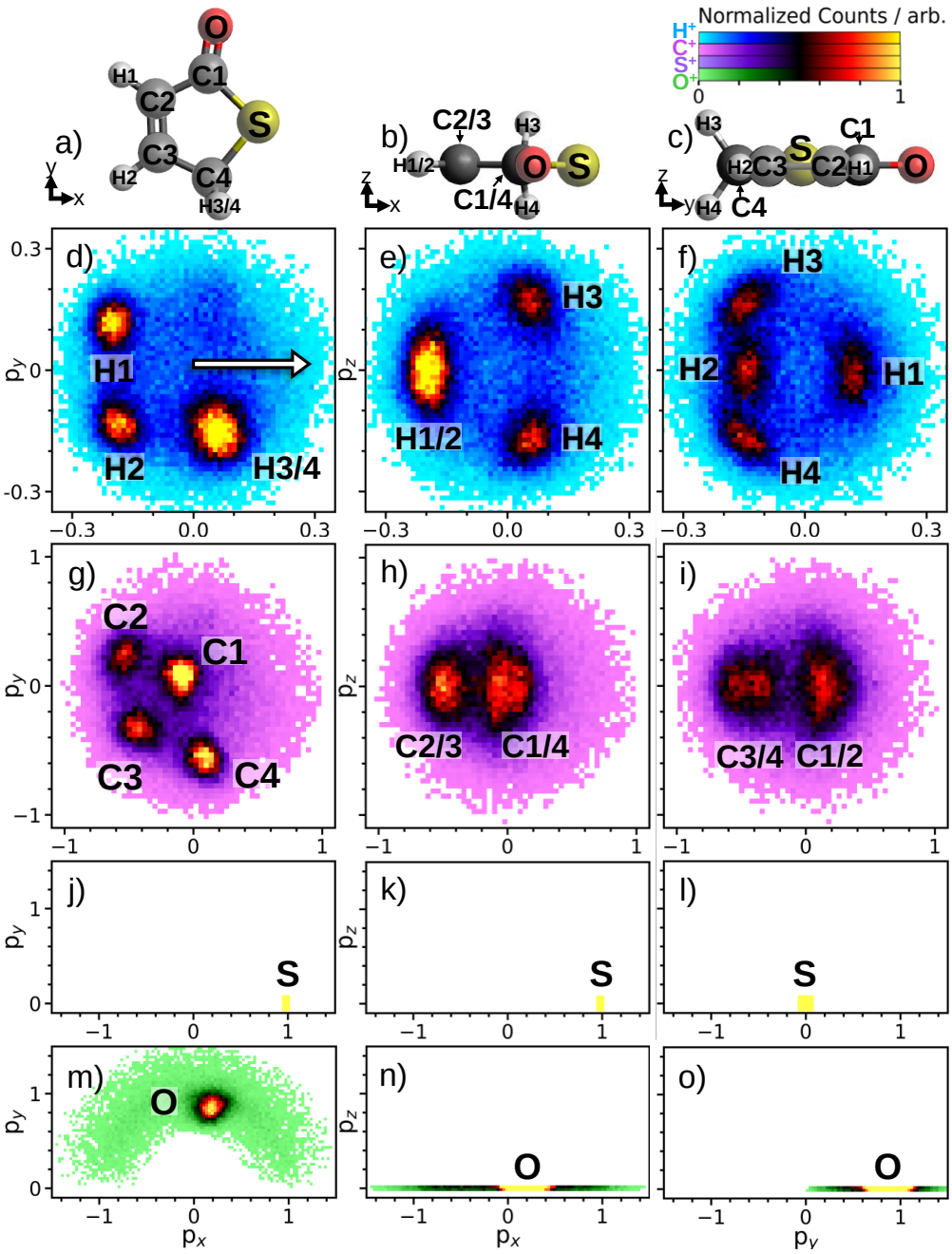

FIG. 2. Newton plots of the coincident momentum distributions of d)-f) H^+, g)-i) C^+, j)-l) S^+, and m)-o) O^+ ions projected onto the xy, xz, and yz planes defined in the same way as in the main text, showing the relative momenta following Coulomb explosion of thiophenone in three dimensions. Ball-and-stick models of thiophenone viewed along three orthogonal axes are displayed in panels a) to c). The counts for H^+, C^+, S^+, and O^+ are normalized independently and are plotted on distinct color scales. As described in the text, the coordinate frame is chosen such that the S^+ momentum points along the positive x axis (see arrow in panel d)) and the O^+ ion momentum spans the xy plane (with p_y ¿ 0). One of these ions or a third particle (H^+ or C^+) is then plotted within this frame and normalized to the momentum of the S^+ ion (see schematic Fig. 1). Therefore in panels j)-o), all S^+ ions have momentum coordinates (1,0,0) and O^+ ions (p_x,p_y > 0,0). Panels a)-i) are reproduced from Fig 2 of the main text.

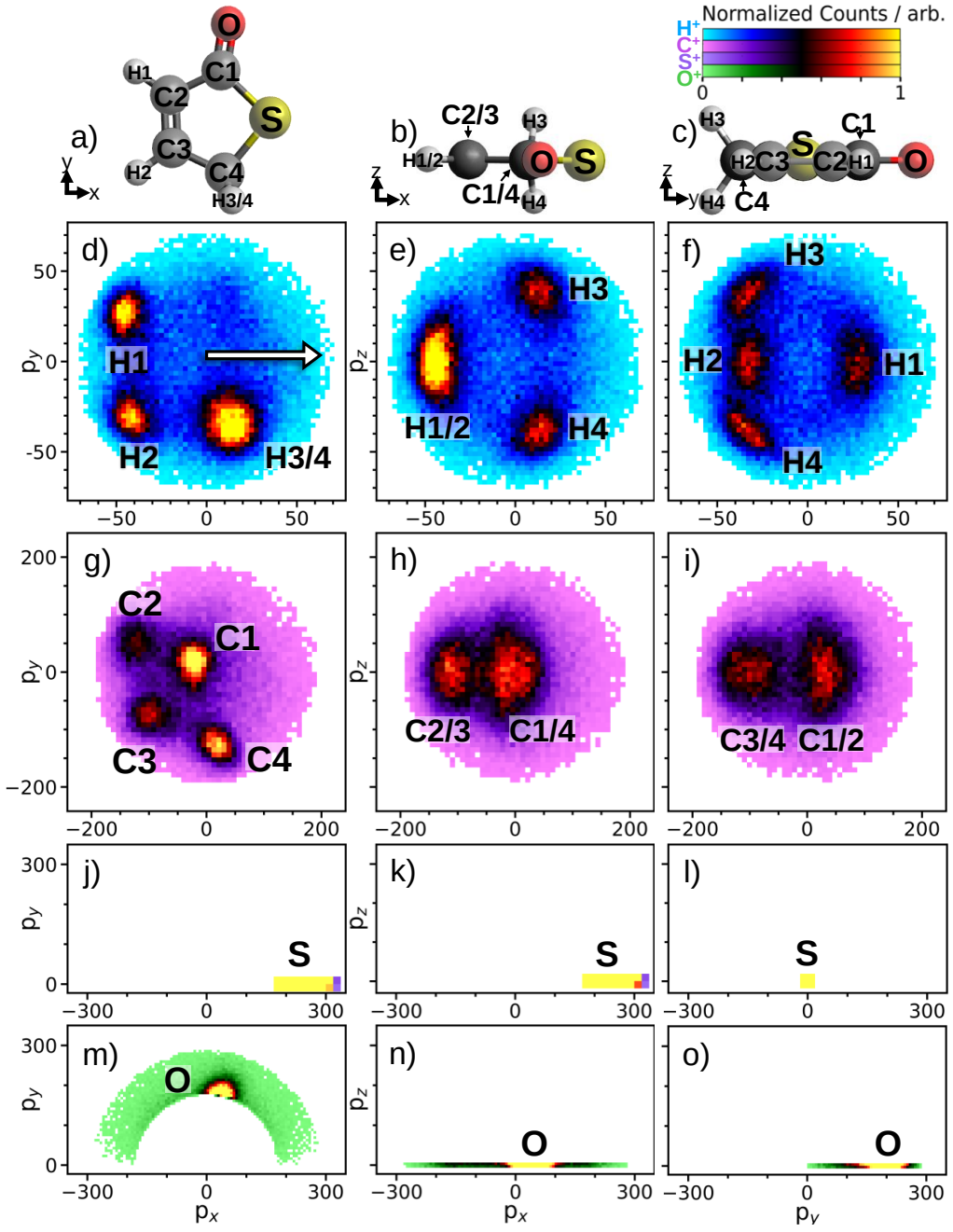

FIG. 3. Newton plots of the coincident momentum distributions of d)-f) H^+, g)-i) C^+, j)-l) S^+, and m)-o) O^+ ions projected onto the xy, xz, and yz planes as in Fig. 2, except momenta are not normalised by the momentum of one of the ions, thus allowing visibility of the spreads in the absolute momenta of the various species. Absolute momenta are calibrated based on the kinetic energy release of $N^+ + N^+$ from Coulomb explision of N_2^{2+} according to Refs. [1, 2].

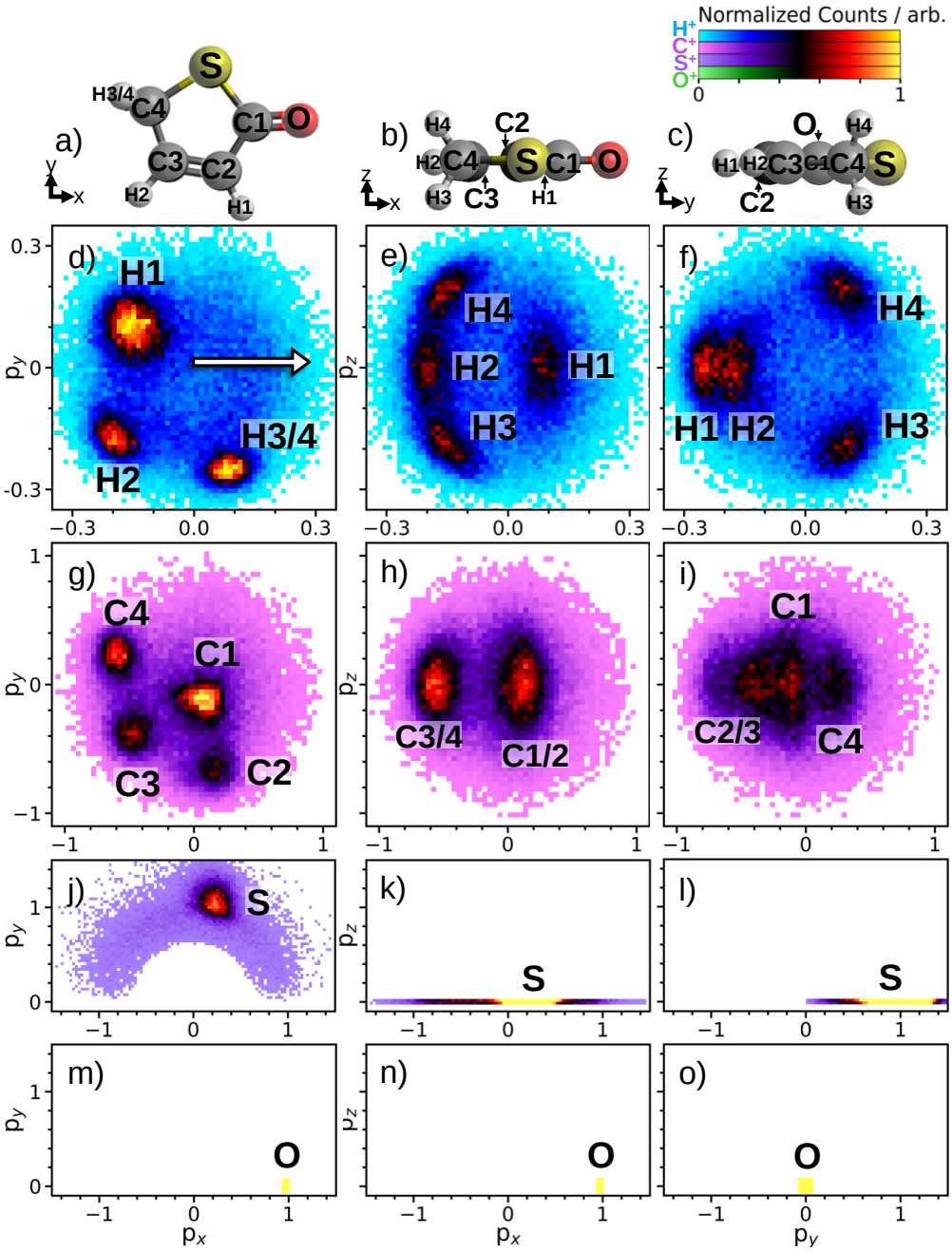

FIG. 4. Newton plots of the coincident momentum distributions of d)-f) H^+, g)-i) C^+, j)-l) S^+, and m)-o) O^+ ions projected onto the xy, xz, and yz planes of an alternative molecular frame to the main text. The alternative coordinate frame, visualized by the ball-and-stick models displayed in panels a) to c), is chosen such that instead the O^+ ion momentum points along the positive x axis (see arrow in panel d), the S^+ ion momentum spans the xy plane (with $p_y > 0$), and one of these ions or a third particle (H^+ or C^+) is plotted within this frame and normalized to the momentum of the O^+. Therefore in panels j)-o), all S^+ ions have momentum coordinates (p_x,$p_y > 0$,0) and O^+ ions (1,0,0).

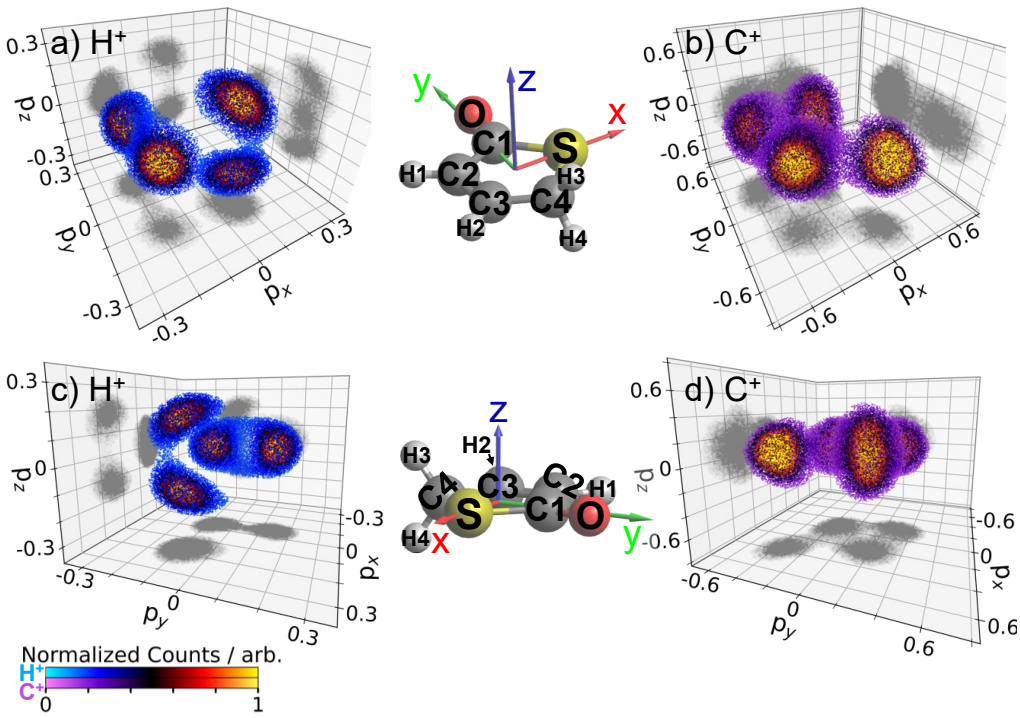

FIG. 5. Three-dimensional scatter representation of experimental a),c) H^+ and b),d) C^+ ion momenta plotted in Cartesian coordinates and viewing the scatter plot from two different directions to give a more visual impression of the three-dimensional nature of the data. Upper and lower insets describe the orientation of the molecule (in these two views) with respect to panels a)-b) and c)-d), respectively. The coordinate frame used is the same as in the main text and is described again in Figs. 1 and 2. The blue/purple to yellow colorscales represent the (separately normalized) density of counts of the H^+/C^+ ions. A limit is imposed for the lowest-density (blue/purple) ions so that the main features are not fully blocked by low-density scatter.

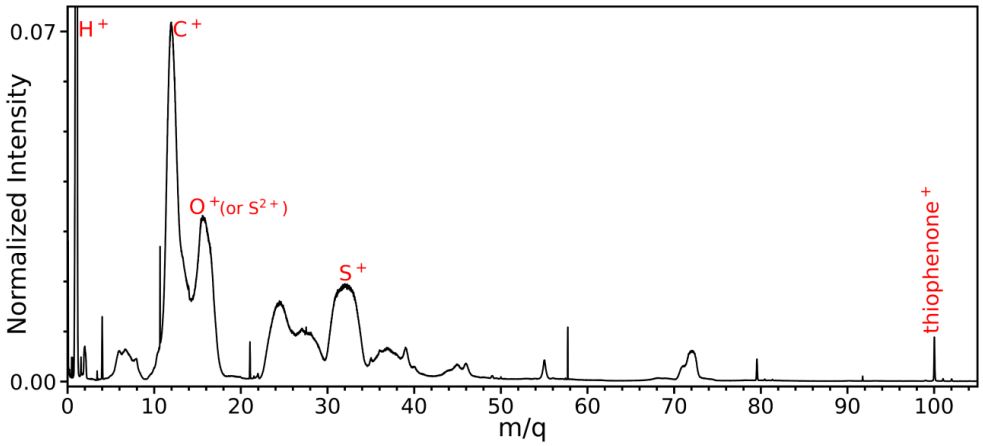

FIG. 6. Time-of-flight mass spectrum of ions recorded with intensity normalized to the maximum of the H^+ peak. Ion hits are histogrammed by their mass-to-charge (m/q) ratio integrating over all x and y dimensions. The parent ions (thiophenone$^+$) along with the atomic ions (H^+, C^+, O^+, S^+) relevant to the main text are labeled in red. Other ions produced from both the sample and background molecules are also present in the spectrum.

II. COULOMB EXPLOSION SIMULATIONS

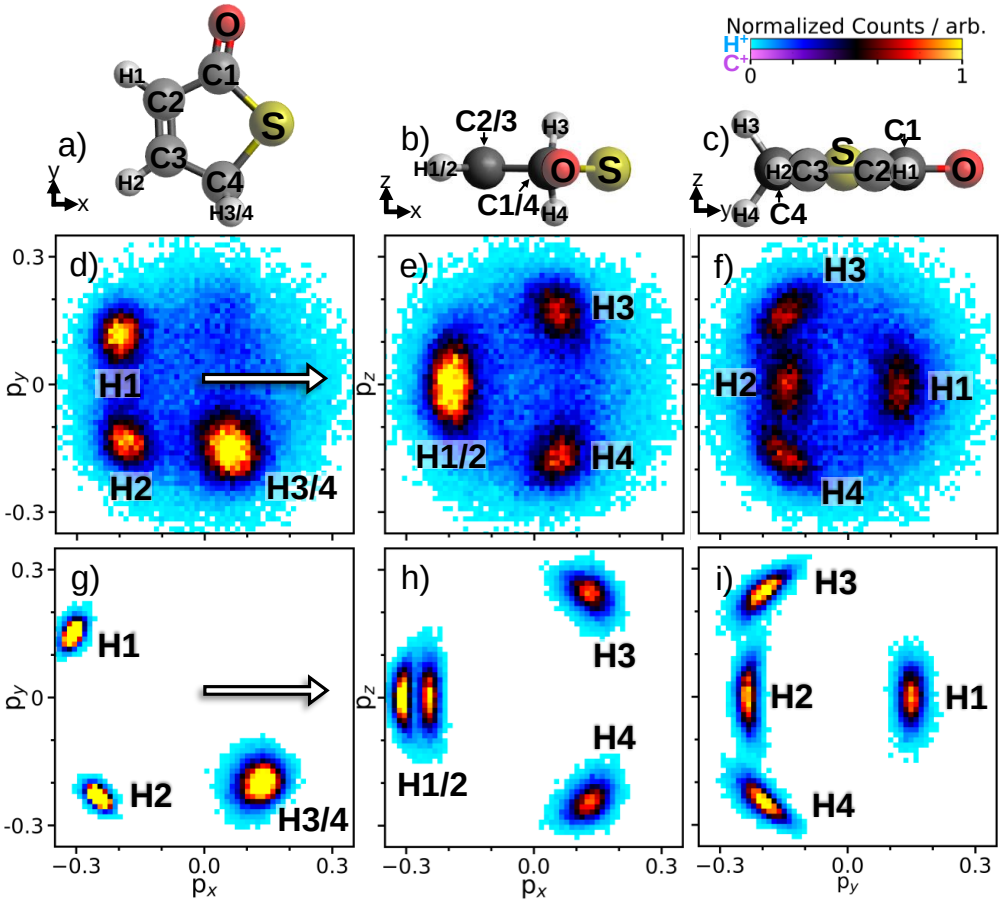

FIG. 7. Direct comparison of d)-f) experimental and g)-i) simulated Newton plots of the normalized coincident momentum distributions of H^+ ions projected onto the xy, xz, and yz planes, the coordinate frame of which is defined in the same way as in the main text and is described again in Figs. 1 and 2. Simulated data are produced using classical Coulomb explosion simulations of a pool of geometries sampled from a Wigner distribution as described in the Methods section. Ball-and-stick models of thiophenone viewed along three orthogonal axes are displayed in panels a) to c). The colorscales are normalized by the total counts. Panels a)-f) are reproduced from Fig. 2 of the main text.

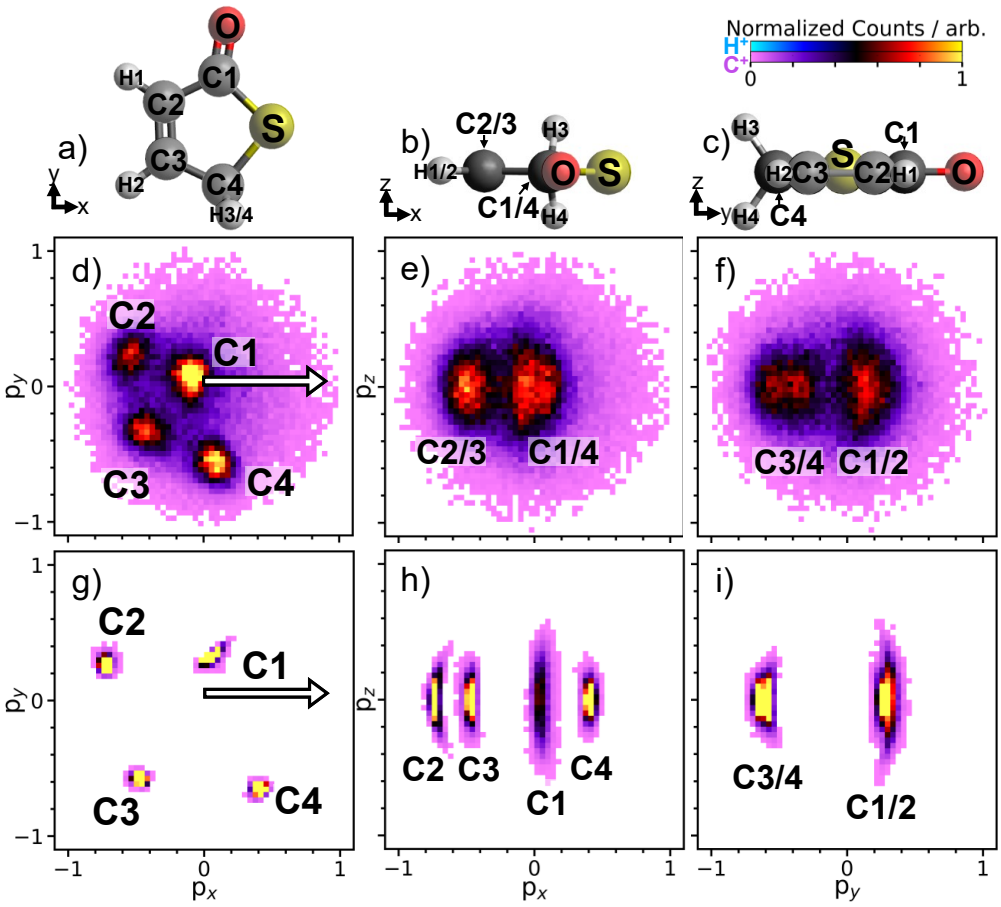

FIG. 8. Same as Fig. 7 but for the coincident momentum distributions of C^+ ions. d)-f) Experimental and g)-i) simulated Newton plots. Ball-and-stick models of thiophenone viewed along three orthogonal axes are displayed in panels a) to c).

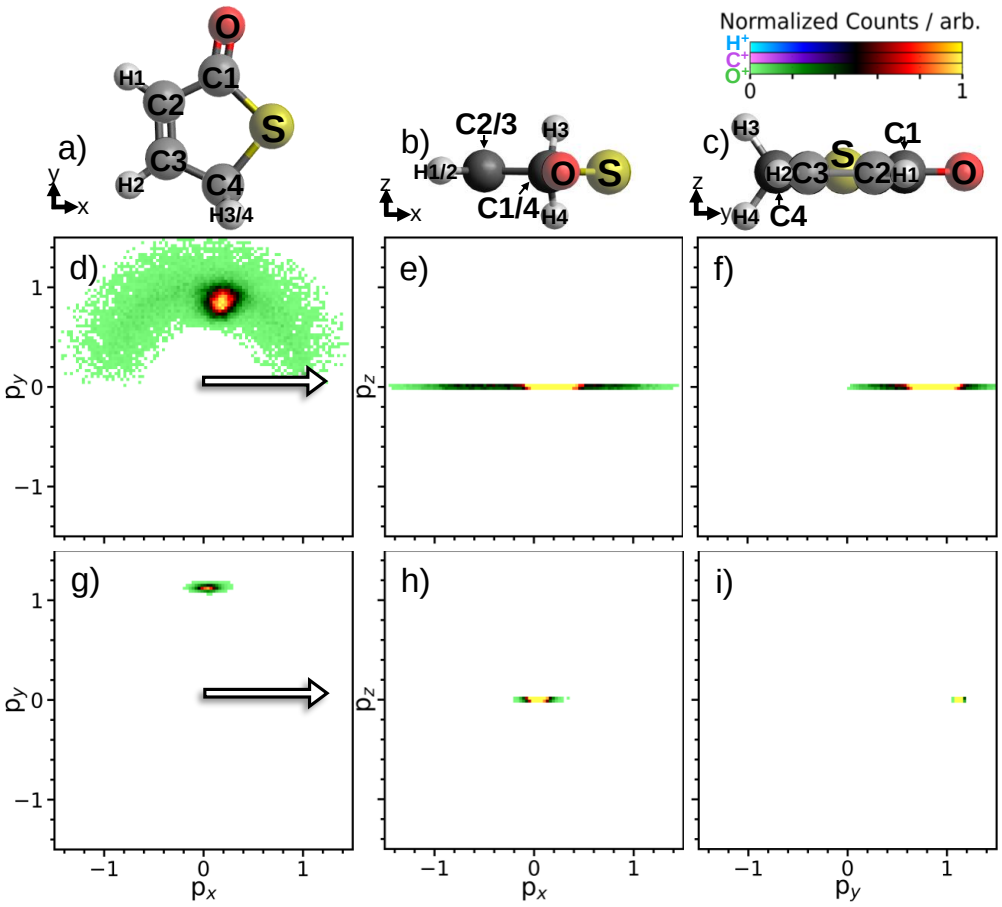

FIG. 9. Same as Fig. 7 but for the coincident momentum distributions of O^+ ions. d)-f) Experimental and g)-i) simulated Newton plots. Ball-and-stick models of thiophenone viewed along three orthogonal axes are displayed in panels a) to c).

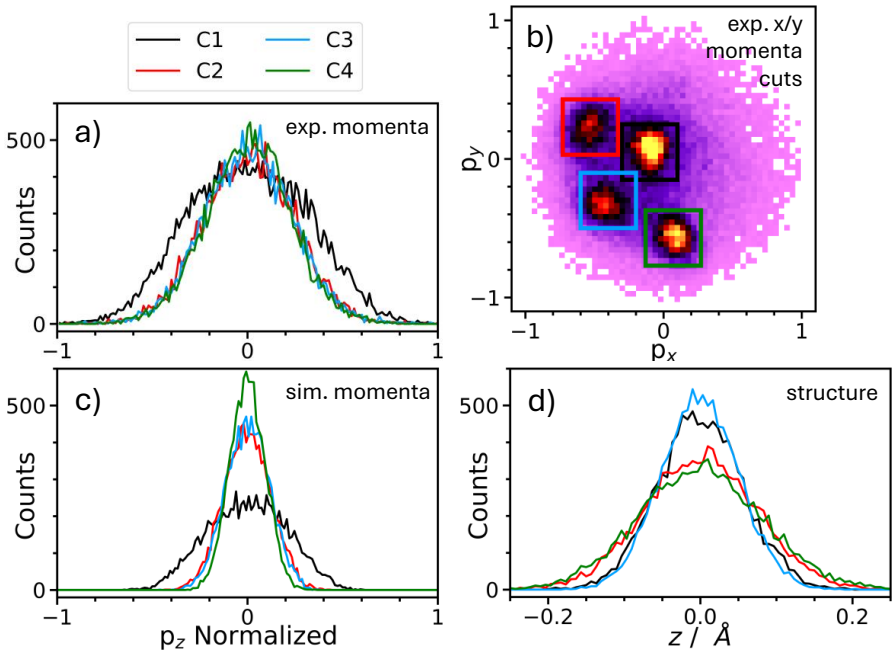

FIG. 10. C^+ ions arising from C1 show a greater spread in momentum in the z-axis (i.e., out of the reference plane). Here, we explore this observation further, both in the experimental data and the simulations. We compare the out-of-plane (z) component of a) experimental momenta, c) simulated momenta, and d) calculated structural position decomposed into the individual carbons (C1-4 as labeled in earlier figures). The definitions of the experimental cuts are given in panel b)Both the experimental and simulated data show that carbons C2, C3, and C4 exhibit a similar spread of z momentum, while C1 shows a significantly broader distribution. Finally, panel d) shows the distribution of real-space out-of-plane positions of each carbon atom in the geometry pool used in the simulation. As the C1 atom does not exhibit a broader spatial distribution, we conclude that the broad momentum distribution associated with the C1 ion is due to specifics of the Coulomb explosion itself (which is reproduced by the simulation).

III. COMPARISON BETWEEN RELATIVE MOMENTA AND MOLECULAR STRUCTURE

One important factor in the interpretation of Coulomb explosion imaging data lies in the relationship between the measured relative ion momenta and the initial structure of the molecule prior to explosion. The experimental images are typically compared to simulations for the explosion of a given structure or pool of structures. Extracting structural parameters (e.g., bond lengths and angles) can also be done within certain limits [3], but this was not necessary for the conclusions drawn in the present manuscript.

To investigate the degree of structural information contained within a Coulomb explosion image, it can be of interest to examine the correlation between experimental (momentum-space) observables and structural parameters. In Fig. 3 of the main text, such a comparison is drawn for the ejection direction of H^+ ions within the molecular frame. Specifically, these are compared to the instantaneous angles of the C-H bonds in the pool of Wigner-sampled geometries. For each geometry, this is done by calculating the angle between each C-H bond and the plane of the heavy atoms (θ), as well as the angle of the C-H bond around the heavy-atom plane (ϕ), where the bisector of the two S-C bonds defines the $+x$ reference vector (where $\phi = \pm 180°$). Comparison is drawn to the angles of the C-H bonds because, in a very simplistic picture, one would expect the H^+ ions to be ejected roughly along the direction of their C-H bond.

For the C^+ ions, drawing comparison to the real-space structure is more complicated, as these atoms lie within the ring of the molecule (closely bonded to two atoms), and thus would not be expected to explode along individual bonds. In Fig. 11, we instead calculate ϕ for each C atom by determining the axis which intersects two adjacent bonds around the thiophene ring. For example, the axis for C1 is defined as the bisector of the C1-S and C1-C2 bonds. The angle between this axis around the molecular plane is then calculated, with the bisector of the two S-C bonds again defining the $+x$ reference vector. For the out-of-plane θ distribution, we calculate the angle between the atomic position of each carbon atom and the heavy-atom plane.

Instead of the above approaches which examine bond axes, one can instead compute angular distributions in polar coordinates based on the atomic coordinates of each atom in a given structure. An example of this is shown in Fig. 12, for both H and C atoms. Here, a coordinate system was used where the origin is the center of mass of the molecule, and the vector between the center of mass and the S atom defines the reference $+x$ vector. This yields generally rather similar distributions to those displayed previously, although the θ angle for the position of out-of-plane hydrogen atoms and the heavy-atom plane is necessarily shallower ($\theta = 90 \pm 20°$) than the angle between each C-H axis and the heavy-atom plane ($\theta = 90 \pm 55°$).

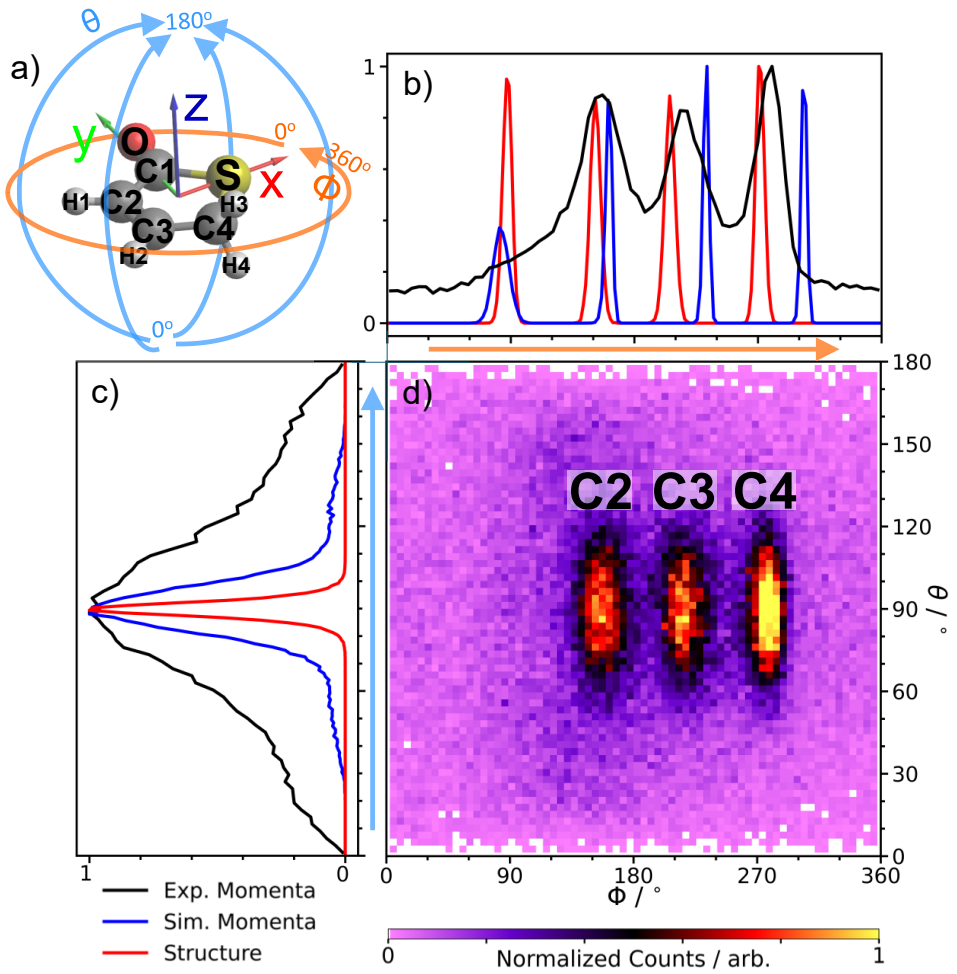

FIG. 11. d) Histogram projecting the density of all C^+ momenta in polar coordinates. a) Angular axes used in panel d) relative to the molecule, defined in the same way as in the main text. b),c) 1D projections of d) onto ϕ and θ. Comparison to Coulomb explosion simulations and bond angles in the real-space structure are also given. The real-space bond angles are calculated using the bisector of the two adjacent bond axes of each carbon atom. The equivalent for H^+ ions is given in Fig. 3 of the main text. Note that in both experiment and simulation, the signature of carbon C1 is less pronounced than the peaks due to carbons C2, C3, and C4 since its momentum is close to zero, which leads to an ill-defined (and thus very broad) momentum angle for the C1 ions. Since the peak width in the experiment is generally broader than in the simulations, C1 only appears as a broad shoulder near $\phi = 90°$.

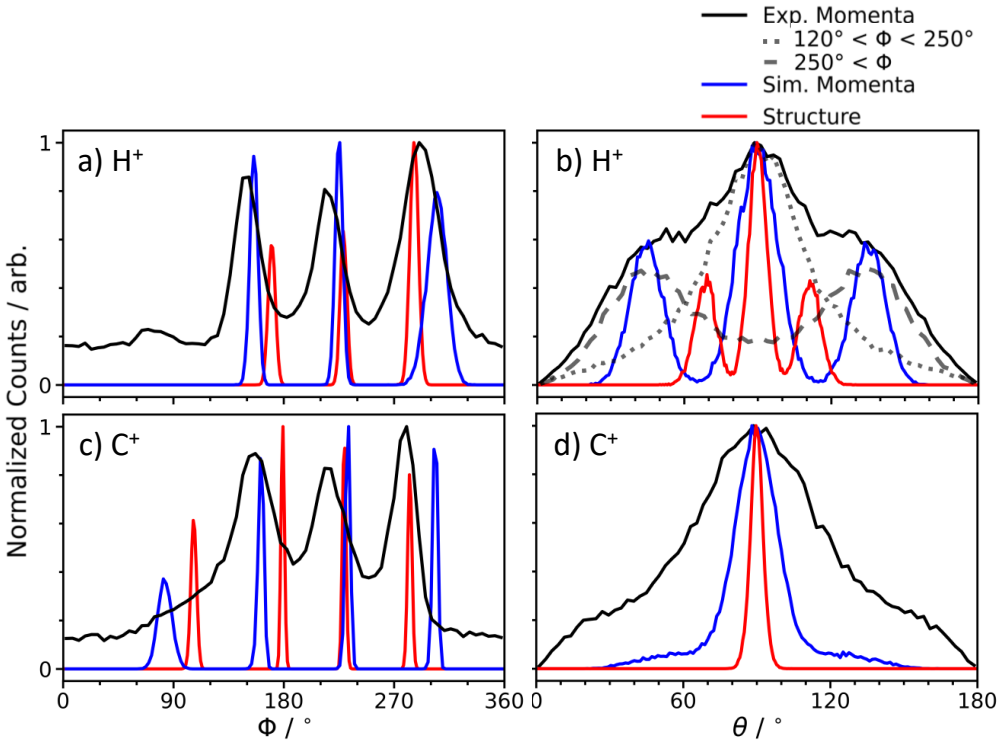

FIG. 12. Experimental (black) and simulated (red) momenta of a)-b) H^+ and c)-d) C^+ ions following Coulomb explosion of thiophenone, projected onto polar coordinates a),c) ϕ and b),d) θ, as also given in Fig. 3 of the main text (H^+) and Fig. 11 (C^+). b) Two slices are shown for the experiment ($120° < \phi < 250°$ or $\phi > 250°$, dot and dash, respectively) - see lines in Fig. 3d of the main text. Comparisons to real-space structure (red) are also given, however this is done in terms of atomic position (instead of bond) relative to the origin at the center of mass.

IV. UV PHOTOCHEMISTRY OF THIOPHENONE

Photoexcitation of thiophenone at around 267 nm populates the optically bright S_2 state, of primarily $n\pi*$ character [4–6]. Nuclear motion along the S-C stretch coordinate enables nonadiabatic relaxation to the S_1 and then S_0 states. This results in the rapid formation of ring-opened biradicals on the S_0 state, with large amounts of excess vibrational energy, which may then undergo subsequent isomerisations. Possible photoreactions are summarized in Fig. 13. These include: ring closing to form either 2(5H)- or 2(3H)-thiophenone; hydrogen migration to yield thioaldehyde or thiol photoproducts, or the formation of a three-membered episulfide ring.

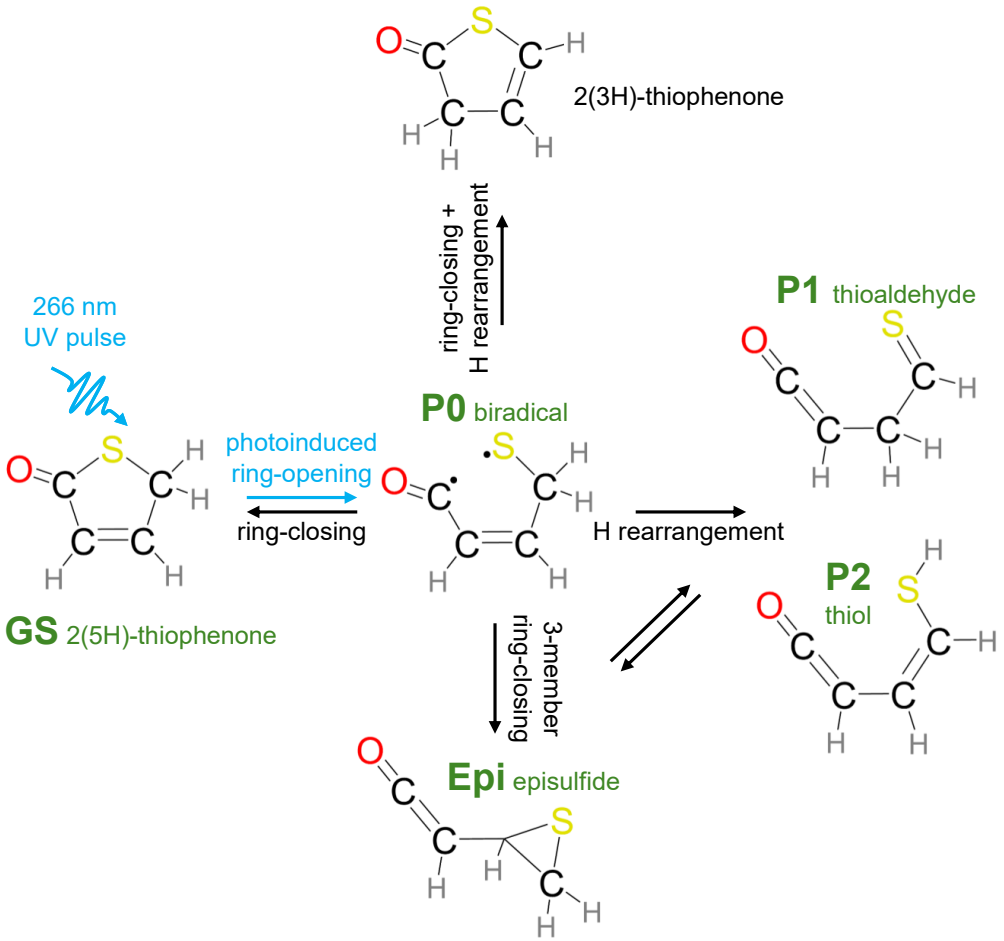

FIG. 13. Reaction scheme illustrating the possible photochemical processes following excitation of thiophenone at 267 nm as reported in previous studies [4–6]. The species selected for Coulomb explosion simulations in Fig. 4 of the main text, to show the potential for CEI to distinguish both a large structural change to a three-membered ring (Epi) but also ring-opened products whose structures differ primarily in the arrangement of hydrogen atoms, are highlighted here by the corresponding green labels. The ring-closing + H rearrangement channel (top) was discounted in Ref. [6] and the other three products concluded to fluctuate between each other. The molecules are given as Lewis structures to emphasise the H atom rearrangements. The main transformations are indicated above the arrows; however, other changes in functionalisation also take place as evinced by the chemical structures.

ALTERNATIVE REPRESENTATIONS OF SIMULATED PHOTOPRODUCTS

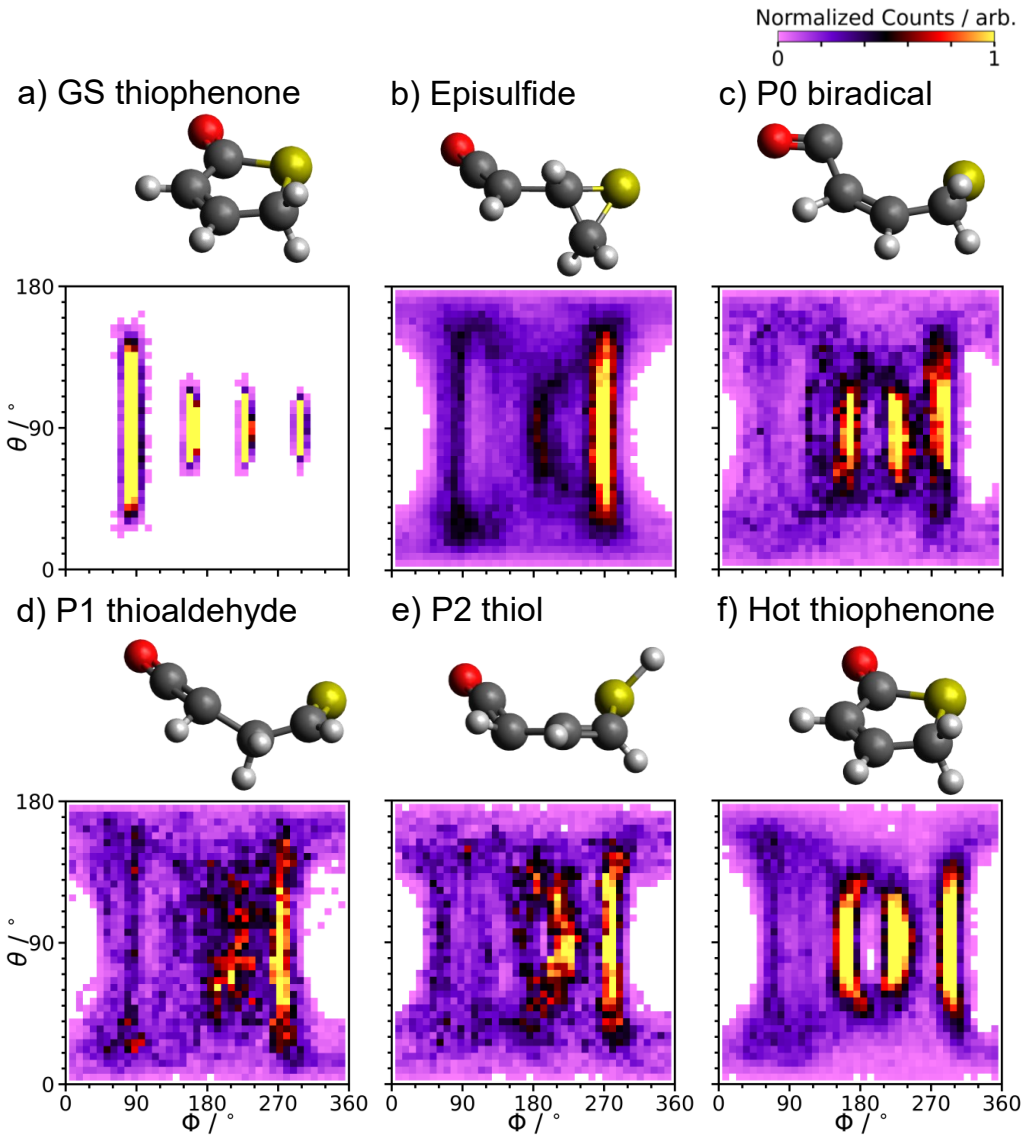

FIG. 14. Same as Fig. 4 of the main text but now showing the three-dimensional C^+ ion momentum distributions (in polar coordinates) predicted for the cold ground state (a) and possible photoproducts of UV-excited thiophenone labeled episulfide (b), P0 (c), P1 (d), P2 (e), and hot thiophenone (f) following prior work [5, 6], as shown by the sketches of the molecular geometry. The coordinate frame used is the same as in the main text and is described again in Figs. 1 and 2. The colorscale is normalized to the number of coincidences contributing to each panel. The *ab initio* molecular dynamics and categorization of the trajectories to the five photoproducts is explained in the Methods section.

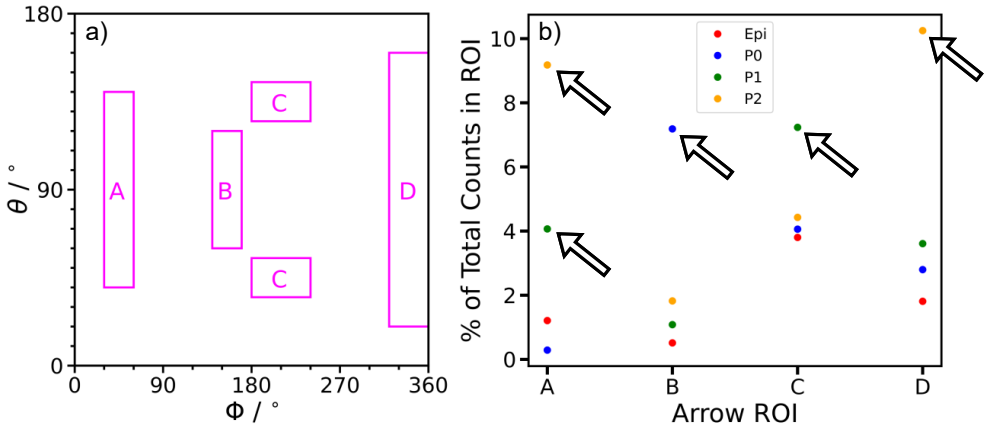

FIG. 15. a) Regions of interest (ROI), using the representation in Fig. 4 of the main text, where simulated signal of ring-opened isomers show significant differences (as highlighted by arrows in Fig. 4). b) Counts from each simulated product in these ROI, as a percentage of the total number of counts for that species in our simulation. It can be seen that different products dominate the signals in these defined ROIs. For instance, in region A, product P2 dominates, with a contribution that is more than twice that of the next strongest contributor (P1) and an order of magnitude (or more) greater than that of the P0 or episulfide (Epi) products. In other regions, the difference between the different photoproducts is less substantial (e.g. region C), however in each case, there is a dominant photoproduct in each ROI.

[1] T. Weber, O. Jagutzki, M. Hattass, A. Staudte, A. Nauert, L. Schmidt, M. Prior, A. Landers, A. Bräuning-Demian, H. Bräuning, et al., K-shell photoionization of CO and N_2: is there a link between the photoelectron angular distribution and the molecular decay dynamics?, Journal of Physics B: Atomic, Molecular and Optical Physics **34**, 3669 (2001).

[2] M. Lundqvist, D. Edvardsson, P. Baltzer, and B. Wannberg, Doppler-free kinetic energy release spectrum of N_2^{2+}, Journal of Physics B: Atomic, Molecular and Optical Physics **29**, 1489 (1996).

[3] X. Li, A. Rudenko, M. Schöffler, N. Anders, T. M. Baumann, S. Eckart, B. Erk, A. De Fanis, K. Fehre, R. Dörner, et al., Coulomb explosion imaging of small polyatomic molecules with ultrashort X-ray pulses, Physical Review Research **4**, 013029 (2022).

[4] D. Murdock, S. J. Harris, J. Luke, M. P. Grubb, A. J. Orr-Ewing, and M. N. Ashfold, Transient UV pump–IR probe investigation of heterocyclic ring-opening dynamics in the solution phase: The role played by nσ^* states in the photoinduced reactions of thiophenone and furanone, Physical Chemistry Chemical Physics **16**, 21271 (2014).

[5] S. Pathak, L. M. Ibele, R. Boll, C. Callegari, A. Demidovich, B. Erk, R. Feifel, R. Forbes, M. Di Fraia, L. Giannessi, et al., Tracking the ultraviolet-induced photochemistry of thiophenone during and after ultrafast ring opening, Nature Chemistry **12**, 795 (2020).

[6] J. P. F. Nunes, L. M. Ibele, S. Pathak, A. R. Attar, S. Bhattacharyya, R. Boll, K. Borne, M. Centurion, B. Erk, M.-F. Lin, et al., Monitoring the evolution of relative product populations at early times during a photochemical reaction, Journal of the American Chemical Society **146**, 4134 (2024).